

Bursting synchronization induced by time-delay excitatory or inhibitory autapse in a minimal neuron-astrocyte network

Liao Yu(余廖), Wenlong Zhu(朱文龙), Zhuoqin Yang(杨卓琴), and Zehan Luo (罗泽翰)
Citation: Chin. Phys. B, 2026, 35 (**6**): 068705. DOI: 10.1088/1674-1056/ae48c2
http://cpb.iphy.ac.cn; http://iopscience.iop.org/cpb

What follows is a list of articles you may be interested in

Dynamical behavior of memristor-coupled heterogeneous discrete neural networks with synaptic crosstalk

Minglin Ma(马铭磷), Kangling Xiong(熊康灵), Zhijun Li(李志军), and Shaobo He(贺少波)
Chin. Phys. B, 2024, 33 (**2**): 028706. DOI: 10.1088/1674-1056/aceee9

Dynamics and synchronization in a memristor-coupled discrete heterogeneous neuron network considering noise

Xun Yan(晏询), Zhijun Li(李志军), and Chunlai Li(李春来)
Chin. Phys. B, 2024, 33 (**2**): 028705. DOI: 10.1088/1674-1056/ad062c

Computational model investigating the effect of magnetic field on neural-astrocyte microcircuit

Li-Cong Li(李利聪), Jin Zhou(周瑾), Hong-Ji Sun(孙洪吉), Peng Xiong(熊鹏), Hong-Rui Wang(王洪瑞), Xiu-Ling Liu(刘秀玲), and Chang-Yong Wang(王常勇)
Chin. Phys. B, 2021, 30 (**6**): 068702. DOI: 10.1088/1674-1056/abea81

Dynamics and coherence resonance in a thermosensitive neuron driven by photocurrent

Ying Xu(徐莹), Minghua Liu(刘明华), Zhigang Zhu(朱志刚), Jun Ma(马军)
Chin. Phys. B, 2020, 29 (**9**): 098704. DOI: 10.1088/1674-1056/ab9dee

Astrocyte and ions metabolism during epileptogenesis: A review for modeling studies

Meng-Meng Du(独盟盟), Jia-Jia Li(李佳佳), Zhi-Xuan Yuan(袁治轩), Yong-Chen Fan(范永晨), Ying Wu(吴莹)
Chin. Phys. B, 2020, 29 (**3**): 038701. DOI: 10.1088/1674-1056/ab6961

SPECIAL TOPIC — Biophysical circuits: Modeling & applications in neuroscience

Bursting synchronization induced by time-delay excitatory or inhibitory autapse in a minimal neuron–astrocyte network

Liao Yu(余廖)[1], Wenlong Zhu(朱文龙)[1], Zhuoqin Yang(杨卓琴)[1,†], and Zehan Luo (罗泽翰)[2]

[1] *School of Mathematical Sciences, Beihang University, Beijing* 100191, *China*
[2] *School of Artificial Intelligence, Beihang University, Beijing* 100191, *China*

(Received 24 December 2025; revised manuscript received 28 January 2026; accepted manuscript online 23 February 2026)

A growing body of research has focused on neuron–astrocyte networks; however, relatively few studies have explored the modulatory role of physiologically relevant time-delayed autapses in such network architectures. In this work, we conduct a preliminary investigation into lag synchronization and phase synchronization of bursting for a pyramidal neuron and an interneuron within a neuron–astrocyte network, which are respectively induced by time delays in excitatory and inhibitory autapses. Our results reveal distinct synchronizations under the regulatory effects of the two types of time-delayed autapses. As the time delay of the excitatory autapses varies, neuronal firing transits from synchronization of the initial bursting through chaotic dynamics and back to synchronized bursting. In contrast, under the modulation of time-delayed inhibitory autapses, the two neurons first exhibit synchronized behaviors across diverse bursting patterns, followed by burst desynchronization. The results uncover the differential regulatory mechanisms of excitatory and inhibitory time-delayed autapses on neuronal synchronization, providing critical empirical evidence for understanding autaptic functions in glia-modulated networks. Moreover, this study lays a solid theoretical foundation for future investigations on autaptic effects in more complex neuron–astrocyte networks and enriches the research landscape of neurodynamics and nonlinear dynamics.

Keywords: astrocyte, time-delayed autapse, bursting, lag synchronization, phase synchronization

PACS: 87.19.lj, 87.19.lm, 87.85.dq

DOI: 10.1088/1674-1056/ae48c2 **CSTR:** 32038.14.CPB.ae48c2

1. Introduction

Electrical activities of neurons are affected by various factors, such as ionic concentration, temperature, and synaptic inputs.[1] Under the action of synapses, neurons receive the electrochemical signals they transmit, and a large number of neuron-synaptic structures form a vast nervous system, thus supporting human activities.[2] In addition to neurons being able to receive such electrochemical signals, astrocytes can also respond to them. Astrocytes are the most widely distributed glial cells in the brain; they can release neurotransmitters to communicate with neurons and play a role in information regulation.[3] Many experiments have shown that astrocytes are involved in information transmission and physiological regulation in the central nervous system. It is therefore imperative to adopt a computationally tractable yet biologically meaningful framework to dissect the complex dynamics of neuron–astrocyte interactions.[39,40]

Zhao *et al.*[4] found that calcium signaling in astrocytes can regulate bursting, among other phenomena, by investigating the role of astrocytes in the kinetic transitions of a minimal neuronal network. The model they employed is not an abstract conjecture but is grounded in experimental evidence of bidirectional neuron–astrocyte regulation and the established paradigm of simplified neural circuit modeling. Furthermore, this simplified architecture has been widely employed to dissect how astrocytes regulate fundamental neural circuit functions via calcium signal dynamics and synaptic feedback loops. For example, Ji *et al.*[5] analyzed bidirectional neuron–astrocyte dynamics and information transfer, highlighting an inspirational role for epilepsy treatment. Different astrocytes at an optimal subthreshold signaling frequency can improve neuronal detection of weak signals.[7,8] Collectively, these studies substantiate the rationality of minimal neuronal networks, enabling them to capture the core features of neuron–astrocyte interactions while elucidating the origins of complex neural dynamics. In addition, Jha *et al.*[6] found that astrocytes and microglia protect neurons from damage in the CNS. A large number of studies have shown that investigating astrocytes can help to better understand brain neural functions[9], such as synaptic formation, metabolic coupling, synaptic transmission, neuronal plasticity, and working memory.[10–13]

Autapses, as self-connecting, ring-shaped synaptic structures,[14] are important self-feedback mechanisms that connect neurons to themselves in different brain regions, as extensively studied in Ref. [15]. Autapses can alter the fre-

†Corresponding author. E-mail: yangzhuoqin@buaa.edu.cn

© 2026 Chinese Physical Society and IOP Publishing Ltd. All rights, including for text and data mining, AI training, and similar technologies, are reserved.

quency of neuronal firing; in particular, excitatory autapses can attenuate neuronal firing.[16,36–38] Fast and slow inhibitory autapses can modulate cluster firing activity.[15] Song *et al.*[17] found that inhibitory autapses inhibit neuronal firing, while excitatory autapses alter firing frequency. Baysal *et al.*[18] studied the phenomenon of autapses achieving chaotic resonance in networks of small-world neurons. Autapses lead to different neuronal firing behaviors[19] and change neuronal synchronization and other behaviors in neuronal networks.[15] Moreover, autapses can cause transitions between resting and cluster firing states.[17] In addition to the aforementioned effects, autapses play a crucial role in the synchronous behavior of coupled neuronal systems in the presence of time delays.[20] Zhang *et al.*[21] investigated the effect of synapses on multiple stochastic resonances in neurons under time delay, showing that synapses and time delay can regulate and control neuronal activity. Parthasarathy *et al.*[22] investigated the role of autapses at different time delays, which significantly affects neuronal synchronization regions and enhances synchronization.

Synchronized neuronal discharges play an important role in neuronal systems, being crucial for information processing and transmission as well as the coordination of motor activities.[23,41] At the same time, synchronized discharges are relevant in some brain disorders; for example, during the onset of epilepsy, certain brain regions exhibit notable neuronal synchronization.[24] The interactions between astrocytes and neurons with autapses are highly complex. Astrocytes can affect neuronal firing behavior by changing intracellular Ca^{2+} concentrations.[4] Studying the role of time-delayed autapses in synchronized firing within neuron–astrocyte networks can therefore better elucidate their role in brain diseases or physiological activities.

In this work, we establish a minimal network comprising a pyramidal (PY) neuron and an interneuron (IN) with time-delayed autapses, coupled to astrocytes, to investigate the effects of excitatory and inhibitory autapse time delays on neuronal bursting behaviors and synchronization between the PY and IN neurons, respectively.

2. Models and methods

2.1. A minimal neuron–astrocyte network model

We consider a minimal neuron–astrocyte network consisting of a PY neuron and an IN coupled to an astrocyte (AS), which is schematically illustrated in Fig. . Here, arrows and dots stand for excitatory and inhibitory effects, respectively. g_{se} denotes the excitatory coupling strength from the PY neuron to the IN neuron, and g_{si} represents the inhibitory coupling strength from the IN neuron to the PY neuron. $\gamma_1 = \gamma_2$ are the coupling strengths of the astrocyte to the two neurons, respectively. g_1 and g_2 indicate the coupling strengths of either the inhibitory or excitatory autapses for the PY and the IN neurons, respectively.

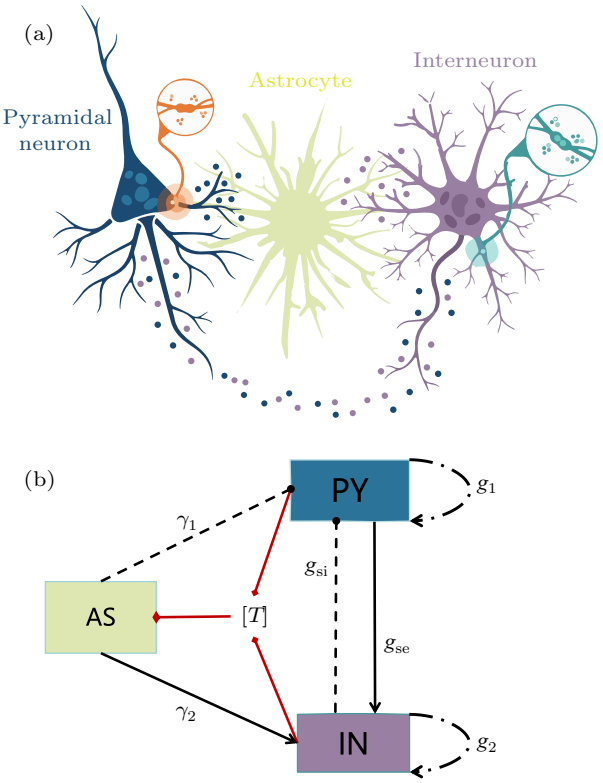


Fig. 1. Schematic architecture of the minimal neuron–astrocyte network model with autapses. The model comprises a PY neuron, an inhibitory IN, and an AS. Solid lines with arrowheads denote excitatory synaptic influences from the PY to the IN neuron, characterized by the gain g_{se} and the astrocytic modulation of the interneuron via γ_2. Dashed lines with dots indicate inhibitory connections, including the feedback inhibition g_{si} from the IN to the PY neuron and astrocytic inhibition of pyramidal activity through γ_1. The red pathways centered on $[T]$ represent the concentration of neurotransmitters released into the synaptic cleft by the neurons, which exert a modulatory effect on the astrocyte. Self-feedback loops, represented by dash-dotted lines, denote autapses g_1 and g_2 within the PY and IN neurons, respectively.

2.1.1. The Morris–Lecar neuron model

Both the PY and IN neurons are modeled using a three-dimensional Morris–Lecar (ML) neuron model,[25] as shown below:

$$C\frac{\mathrm{d}V_j}{\mathrm{d}t} = I_j(t) + I_j^{\mathrm{ext}}(t) + g_{\mathrm{Ca}}M_\infty(V_j)(V_{\mathrm{Ca}} - V_j) + g_{\mathrm{K}}W_j(t)(V_{\mathrm{K}} - V_j) + g_{\mathrm{L}}(V_{\mathrm{L}} - V_j), \quad (1)$$

$$\frac{\mathrm{d}W_j}{\mathrm{d}t} = \tau_W(V_j)[W_\infty(V_j) - W_j], \quad (2)$$

$$\frac{\mathrm{d}I_j^{\mathrm{ext}}}{\mathrm{d}t} = \varepsilon(V_0 - V_j) + \mu I_j^{\mathrm{ext}}, \quad (3)$$

with

$$M_\infty(V_j) = 0.5\left[1 + \tanh\left(\frac{V_j - V_1}{V_2}\right)\right], \quad (4)$$

$$W_\infty(V_j) = 0.5\left[1 + \tanh\left(\frac{V_j - V_3}{V_4}\right)\right], \quad (5)$$

$$\tau_W(V_j) = \frac{1}{\cosh\left(\frac{V_j - V_3}{2V_4}\right)}, \tag{6}$$

$$I_j(t) = I_j^{\rm syn}(t) + I_j^{\rm ast}(t) + I_j^{\rm aut}(t). \tag{7}$$

Here, $V_j(t)$ and $W_j(t)$ represent the membrane potential and the opening probability of the voltage-gated K^+ channel for neuron j, respectively, where j denotes PY or IN. $I_j(t)$ is the sum of the currents generated by neuron j in response to neuronal coupling, astrocytes, and autapses, where $I_j^{\rm syn}(t)$ is the synaptic coupling current, $I_j^{\rm ast}(t)$ is the astrocytic current, and $I_j^{\rm aut}(t)$ is the autaptic current. The external current $I_j^{\rm ext}(t)$ is treated as a dynamic variable governed by Eq. (3) to produce rich cluster firing and chaotic dynamics. $M_\infty(V_j)$ and $W_\infty(V_j)$ are the steady-state opening probabilities of the calcium and potassium ion channels, respectively, and $\tau_W(V_j)$ is the rate constant for the opening of the potassium channel.

The coupled interaction between the two neurons is constructed following Ref. [26]:

$$\frac{{\rm d}g_j}{{\rm d}t} = \alpha_{\rm s}[T]_j(t)[1 - g_j(t)] - \beta_{\rm s} g_j(t), \tag{8}$$

where g_j denotes the open proportion of receptor channels on neuron j, and $\alpha_{\rm s}$ and $\beta_{\rm s}$ are the forward and backward binding rate constants of neurotransmitter concentration $[T]_j$ to open the receptors.

The concentration of neurotransmitter $[T]_j$ in the synaptic cleft by neuron j is expressed as[26]

$$[T]_j(t) = \frac{1}{1 + \exp(-(V_j(t) - \theta_{\rm s})/\sigma_{\rm s})}, \tag{9}$$

where $\theta_{\rm s}$ and $\sigma_{\rm s}$ are the half-activation voltage and steepness of the sigmoid function, respectively.

Consequently, the synaptic currents are expressed as[26]

$$I_{\rm PY}^{\rm syn}(t) = -g_{\rm si}(V_{\rm PY} - V_{\rm si})g_{\rm IN}(t), \tag{10}$$

$$I_{\rm IN}^{\rm syn}(t) = -g_{\rm se}(V_{\rm IN} - V_{\rm se})g_{\rm PY}(t). \tag{11}$$

2.1.2. Astrocyte model

The regulatory effect of astrocytes on neurons is primarily mediated by IP_3, which modulates Ca^{2+} channels, thereby affecting cytosolic Ca^{2+} concentration and neuronal firing. The dynamics of IP_3 are described by[27]

$$\frac{{\rm d}[{\rm IP_3}]}{{\rm d}t} = \frac{[{\rm IP_3^*}] - [{\rm IP_3}]}{\tau_{\rm IP_3}} + r_{\rm IP_3}([T]_{\rm PY} + [T]_{\rm IN}), \tag{12}$$

where $[{\rm IP_3^*}]$ is the equilibrium concentration of IP_3, $\tau_{\rm IP_3}$ is a time constant, and $r_{\rm IP_3}$ is the conversion factor for neuronal transmitter concentration to IP_3.

The variation of cytosolic Ca^{2+} concentration, $[Ca^{2+}]$, is described by the classical Li–Rinzel model[28]

$$\frac{{\rm d}[{\rm Ca^{2+}}]}{{\rm d}t} = J_{\rm chan} - J_{\rm pump} + J_{\rm leak}, \tag{13}$$

$$\frac{{\rm d}q}{{\rm d}t} = \alpha_q(1 - q) - \beta_q q. \tag{14}$$

Thus, the astrocyte coupling model is constructed using Eqs. (12)–(14), where $[Ca^{2+}]$ evolves in time, and q is the fraction of activated IP_3 receptors. The terms $J_{\rm chan}$, $J_{\rm pump}$, and $J_{\rm leak}$ represent the calcium flux from the ER to cytosol, the pump flux from cytosol to ER, and the leakage flux from ER to cytosol, respectively, with $[Ca^{2+}]_{\rm ER}$ the calcium concentration in the ER.

$$J_{\rm chan} = c_1 v_1 p_\infty^3 n_\infty^3 q^3([{\rm Ca^{2+}}]_{\rm ER} - [{\rm Ca^{2+}}]), \tag{15}$$

$$J_{\rm pump} = \frac{v_3[{\rm Ca^{2+}}]^2}{[{\rm Ca^{2+}}]^2 + k_3^2}, \tag{16}$$

$$J_{\rm leak} = c_1 v_2([{\rm Ca^{2+}}]_{\rm ER} - [{\rm Ca^{2+}}]), \tag{17}$$

$$p_\infty = \frac{[{\rm IP_3}]}{[{\rm IP_3}] + d_1}, \tag{18}$$

$$n_\infty = \frac{[{\rm Ca^{2+}}]}{[{\rm Ca^{2+}}] + d_4}, \tag{19}$$

$$\alpha_q = a_1 d_2 \frac{[{\rm IP_3}] + d_1}{[{\rm IP_3}] + d_3}, \tag{20}$$

$$\beta_q = a_1[{\rm Ca^{2+}}], \tag{21}$$

$$[{\rm Ca^{2+}}]_{\rm ER} = \frac{c_0 - [{\rm Ca^{2+}}]}{c_1}. \tag{22}$$

When $[Ca^{2+}]$ in astrocytes reaches a threshold, neurotransmitters are released to neurons, where Θ is the Heaviside function[27]

$$I_j^{\rm ast}(t) = 2.11\Theta(\ln y)\ln y, \tag{23}$$

with $y(t) = [Ca^{2+}] - 196.69$.

Table 1. Corresponding values of all fixed parameters.

Parameters	values	Parameters	values
C	20 μF/cm^2	$g_{\rm s}$	3 mS/cm^2
$V_{\rm Ca}$	120 mV	$g_{\rm Ca}$	4 mS/cm^2
$V_{\rm K}$	−84 mV	$g_{\rm K}$	8 mS/cm^2
$V_{\rm L}$	−60 mS/cm^2	$g_{\rm L}$	2 mS/cm^2
V_0	−20 mV	V_1	−1.2 mV
V_2	18 mV	V_3	13 mV
V_4	17.4 mV	a	0.005
μ	0.0001	ϕ	0.23
$\theta_{\rm s}$	20 mV	$\sigma_{\rm s}$	2 mV
$\alpha_{\rm s}$	1.1	$\beta_{\rm s}$	0.19
$\gamma_{\rm h}$	10 mV	d_2	0.13 μm
$V_{\rm si}$	−80 mV	$V_{\rm se}$	20 mV
c_0	2 μm	c_1	0.185
v_1	6 s^{-1}	v_1	0.11 s^{-1}
d_1	0.13 μm	d_2	1.049 μm
d_3	0.9434 μm	d_4	0.082 μm
a_1	0.2 s^{-1}	τ_{ip_3}	7 s
r_{ip_3}	0.72 s^{-1}	$[{\rm IP_3^*}]$	0.16 μm

2.1.3. Autapse model

The chemical autapse with time delay τ is described by

$$I_j^{\rm aut}(t) = -g_j(V_j - E_{\rm s}) - F(V_j(t-\tau)), \tag{24}$$

$$F(V_j(t-\tau)) = \frac{1}{1+\exp[-10(V_j(t-\tau) - V_{\rm thres})]}, \tag{25}$$

where $V_{\rm thres}$, the synaptic threshold, is set at -10 mV, such that V_j crossing this threshold can activate the autaptic current.[16]

Overall, the minimal network integrates astrocyte and autapse interactions in the PY and IN neurons, with the fixed values of all parameters[29] listed in Table 1.

2.2. Quantification of lag synchronization and phase synchronization

In recent years, an increasing number of synchronization phenomena have been reported in neuronal networks and coupled neurons, such as complete synchronization,[30] cluster synchronization,[31] phase synchronization,[32] and lag synchronization.[33] These synchronizations are also related to the progression of various nervous system diseases, including Alzheimer's disease and Parkinson's disease, making it meaningful to study synchronization phenomena in coupled neuronal networks.[34] Among the aforementioned types, lag synchronization and phase synchronization are specifically examined using the following approaches.

2.2.1. Lag synchronization

Lag synchronization occurs when the firing states of two neurons are nearly identical but consistently delayed relative to each other. To quantify lag synchronization, the cross-correlation function (CCF) is employed

$$\mathrm{Corr}(\Delta t) = \frac{\sum_t [X_{\rm PY}(t) - \bar{X}_{\rm PY}][X_{\rm IN}(t+\Delta t) - \bar{X}_{\rm IN}]}{\sqrt{\sum_t [X_{\rm PY}(t) - \bar{X}_{\rm PY}]^2 \sum_t [X_{\rm IN}(t) - \bar{X}_{\rm IN}]^2}}, \tag{26}$$

where the lag Δt is determined from the maximum value of $\mathrm{Corr}(\Delta t)$. To further verify lag synchronization, the time series of the IN neuron is shifted by Δt (added if $\Delta t > 0$, subtracted if $\Delta t < 0$) to align temporally with the PY neuron. The quantitative criteria for lag synchronization are defined as follows: (i) complete lag synchronization: $|\max(\mathrm{Corr}(\Delta t))| \geq 0.9$; (ii) incomplete lag synchronization: $0.7 \leq |\max(\mathrm{Corr}(\Delta t))| < 0.9$; (iii) no lag synchronization: $|\max(\mathrm{Corr}(\Delta t))| < 0.7$, with no meaningful temporal alignment.

2.2.2. Phase synchronization

Phase synchronization is characterized by whether the phase difference between two signals remains stable (constant or periodically varying). The Hilbert transform is applied to neuronal signals $V_{\rm PY}$ and $V_{\rm IN}$ to obtain instantaneous phases $\varphi_j(t)$ via phase unwrapping [35]

$$Z_j(t) = X_j(t) + \mathrm{i}H[X_j(t)], \tag{27}$$

$$\varphi_j(t) = \arctan\left(\frac{H[X_j(t)]}{X_j(t)}\right), \quad j = \mathrm{PY}, \mathrm{IN}. \tag{28}$$

The phase difference is then

$$\Delta\varphi(t) = \varphi_{\rm PY}(t) - \varphi_{\rm IN}(t) \mod 2\pi. \tag{29}$$

The phase locking value (PLV) is computed as

$$\mathrm{PLV} = \left| \frac{1}{N} \sum_{t=1}^{N} \mathrm{e}^{\mathrm{i}\Delta\varphi(t)} \right|, \tag{30}$$

where N is the number of iterations and $\mathrm{i}^2 = -1$. PLV approaching 1 indicates strong phase synchronization, near 0 signifies no synchronization, and around 0.5 corresponds to moderate synchronization, which should be interpreted alongside other metrics.

All numerical simulations are implemented in MATLAB R2021a (MathWorks, USA). Nonlinear differential equations are integrated using a standard fourth-order Runge–Kutta algorithm with a fixed time step of $\Delta t = 1$ ms. Initial conditions are set to the steady-state values under input-free conditions. To remove transient effects, an initial period of 100 s is discarded, and all statistical metrics, including the cross-correlation function and PLV, are computed over a stable 100 s simulation window.

3. Time-delay autapse evokes lag and phase synchronizations of bursting in the neuron–astrocyte network

To investigate neuronal firing transitions under delayed autapses, synchronization levels are quantified using both PLV and maximum cross-correlation as functions of the autaptic time delay τ. As illustrated in Fig. 2(a), both excitatory and inhibitory autapses show a non-monotonic dependence of phase synchronization on τ. For excitatory autapses, high phase locking occurs at very short delays, followed by a desynchronization window for 100 ms $< \tau <$ 300 ms. Beyond this interval, the PLV gradually recovers and stabilizes. In contrast, the inhibitory autapse exhibits a phase-shifting property: a sharp dip at $\tau < 50$ ms, while robust phase locking persists across longer delays. This suggests the inhibitory autapse is more effective at maintaining phase coherence under substantial delays.

Analysis of lag synchronization in Fig. 2(b) reveals a complex, non-monotonic dependence on τ. The excitatory autapse shows high synchronization at minimal delays and for $\tau >$ 400 ms, but exhibits a desynchronization window for 100 ms $< \tau <$ 300 ms. The inhibitory autapse maintains high lag synchronization with only a localized dip near $\tau \approx 100$ ms before recovering at higher delays. These results suggest inhibitory autaptic currents are more resilient in preserving temporal precision, whereas excitatory autaptic currents are more susceptible to delay-induced disruption. Subsequent sections discuss specific autaptic types and time delays in detail.

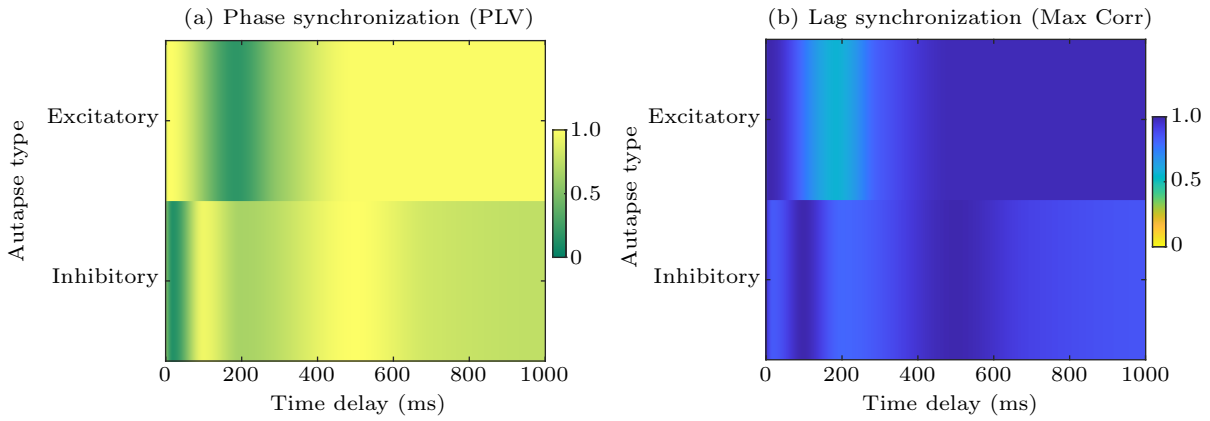


Fig. 2. Influence of autaptic type and time delay τ on synchronization dynamics. (a) Heatmap of PLV as a function of time delay τ (0–1000 ms) for excitatory and inhibitory autapses. (b) Corresponding lag synchronization, quantified by the maximum cross-correlation, across the same parameter space.

3.1. Synchronization of bursting induced by non-synchronized chaos due to time delay of excitatory autapse

We investigate excitatory autapse by introducing the autaptic current $I_j^{\mathrm{aut}}(t)$ $(j = \mathrm{PY}, \mathrm{IN})$ in Eq. (7). Here, we set $E_{\mathrm{s}} = 30$ mV in Eq. (24), exceeding the minimum voltage during neuronal firing, to examine how excitatory autapses affect firing patterns in the neuron–astrocyte network. The coupling strengths are set to $g_{\mathrm{se}} = g_{\mathrm{si}} = g = 0.5$, with astrocytic modulation strengths $\gamma_1 = \gamma_2 = \gamma = 0.9$ for the PY and IN neurons, respectively. The autaptic time delay τ is varied over 0 ms, 10 ms, 186 ms, 300 ms, and 500 ms to explore its effects on lag synchronization (via Δt from the maximum of $\mathrm{Corr}(\Delta t)$), phase synchronization (via phase difference and PLV), and neuronal firing patterns (via power spectral density, PSD) at different frequencies.

At $\tau = 0$ ms, both PY and IN neurons, driven by positive autaptic currents, exhibit bursting behavior characterized by lag synchronization, as depicted in Fig. 3(a). The excitatory autaptic currents I_j^{aut} for both neurons remain positive (facilitating firing) during bursts and drop to zero at burst termination. The computed lag is $\Delta t = 0.4887$ s from the maximum of $\mathrm{Corr}(\Delta t)$ in Eq. (26). By shifting the IN neuron time series as $V_{\mathrm{IN}}(t) = V_{\mathrm{IN}}(t + 0.4887)$, the two neuronal time series overlap

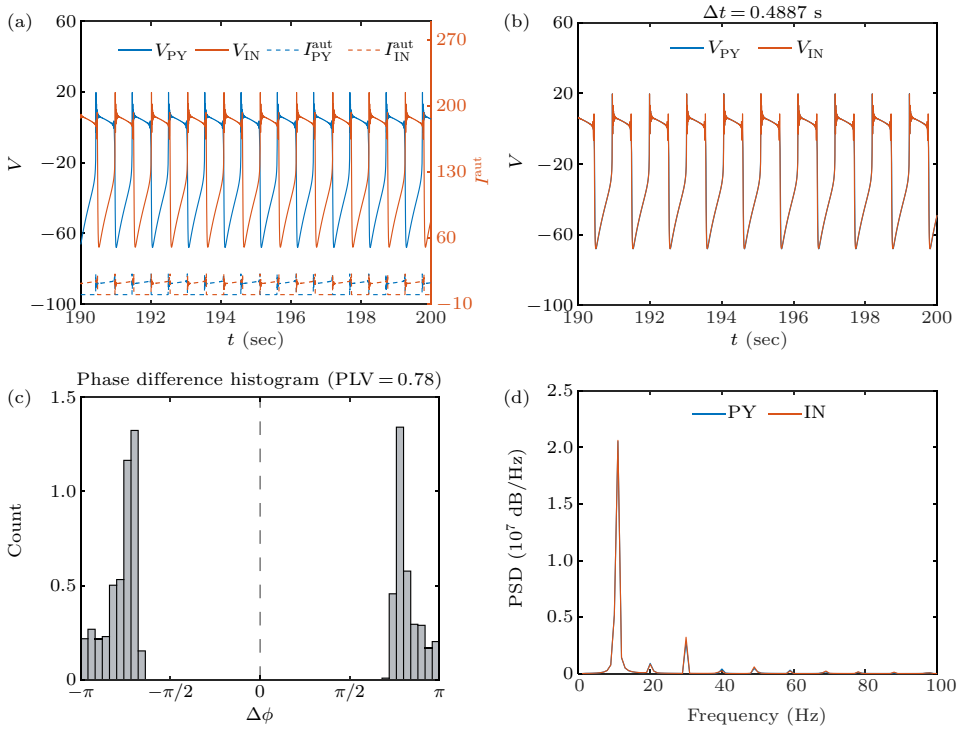


Fig. 3. Lag and phase synchronizations at the time delay $\tau = 0$ ms for the excitatory autapse in the neuron–astrocyte network. (a) Time series of membrane potentials (V_{PY}, V_{IN}, solid lines) and corresponding autaptic currents ($I_{\mathrm{PY}}^{\mathrm{aut}}$, $I_{\mathrm{IN}}^{\mathrm{aut}}$, dashed lines) for the PY neuron (blue lines) and IN (orange lines), where both neurons exhibit bursting behavior. (b) Temporal alignment of neuronal membrane potentials following a compensatory shift of $\Delta t = 0.4887$ s, corresponding to the lag at which the cross-correlation function is maximized. After alignment, the two neurons exhibit nearly overlapping bursts, confirming lag synchronization between PY and IN neurons. (c) Histogram showing the distribution of phase differences ($\Delta\varphi$) between PY and IN neurons. The PLV of 0.78 indicates the presence of phase synchronization. (d) Coinciding PSD curves for the PY and IN neurons reveal nearly identical dominant frequencies.

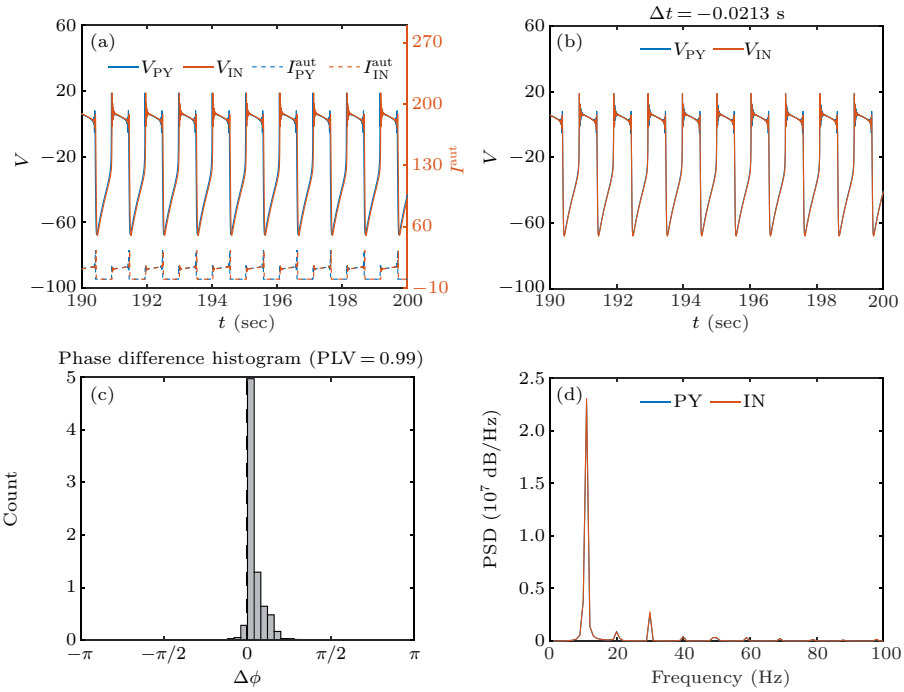


Fig. 4. Lag and phase synchronizations at the time delay $\tau = 10$ ms for the excitatory autapse in the neuron–astrocyte network. (a) Time series of membrane potentials (V_{PY}, V_{IN}, solid lines) and corresponding autaptic currents (I^{aut}_{PY}, I^{aut}_{IN}, dashed lines) for the PY neuron (blue lines) and IN (orange lines). The two neurons exhibit nearly complete synchronous bursting. (b) Temporal alignment of neuronal membrane potentials following a compensatory shift of $\Delta t = -0.0213$ s. The precise overlap of the traces demonstrates nearly complete synchronization. (c) Histogram showing the distribution of phase differences ($\Delta\varphi$) between PY and IN neurons. The sharp clustering of $\Delta\varphi$ near zero, together with a PLV of 0.99, indicates robust phase synchronization. (d) PSD curves for the PY and IN neurons as a function of frequency. The overlapping curves further validate synchronous bursting.

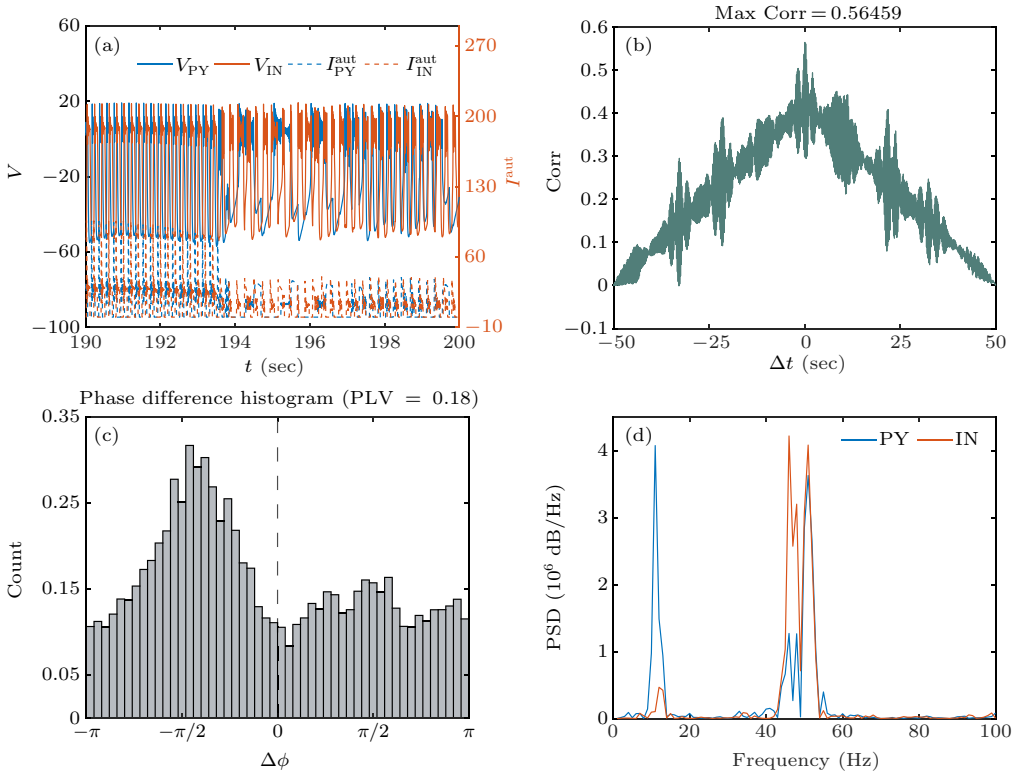


Fig. 5. No synchronization due to chaotic bursting at the time delay $\tau = 186$ ms for the excitatory autapse in the neuron–astrocyte network. (a) Time series of membrane potentials (V_{PY}, V_{IN}, solid lines) and corresponding autaptic currents (I^{aut}_{PY}, I^{aut}_{IN}, dashed lines) for the PY neuron (blue lines) and IN (orange lines). For both neurons, the autaptic currents exhibit irregular fluctuations, and the membrane potentials display chaotic bursting patterns. (b) The cross-correlation Corr(Δt) quantifies the degree of lag synchronization. The peak value reaches approximately 0.56459, indicating a lack of robust temporal alignment between PY and IN neurons. (c) Histogram showing the distribution of phase differences ($\Delta\varphi$) between PY and IN neurons. The distribution is notably broad and non-uniform, yielding a PLV of 0.18. The absence of a prominent peak at $\Delta\varphi = 0$ confirms that the system operates in a desynchronized regime characterized by disordered phase relationships. (d) PSD curves for the PY and IN neurons. The divergence of primary spectral peaks, alongside the emergence of broadband noise, underscores the chaotic nature of the firing and the breakdown of frequency entrainment.

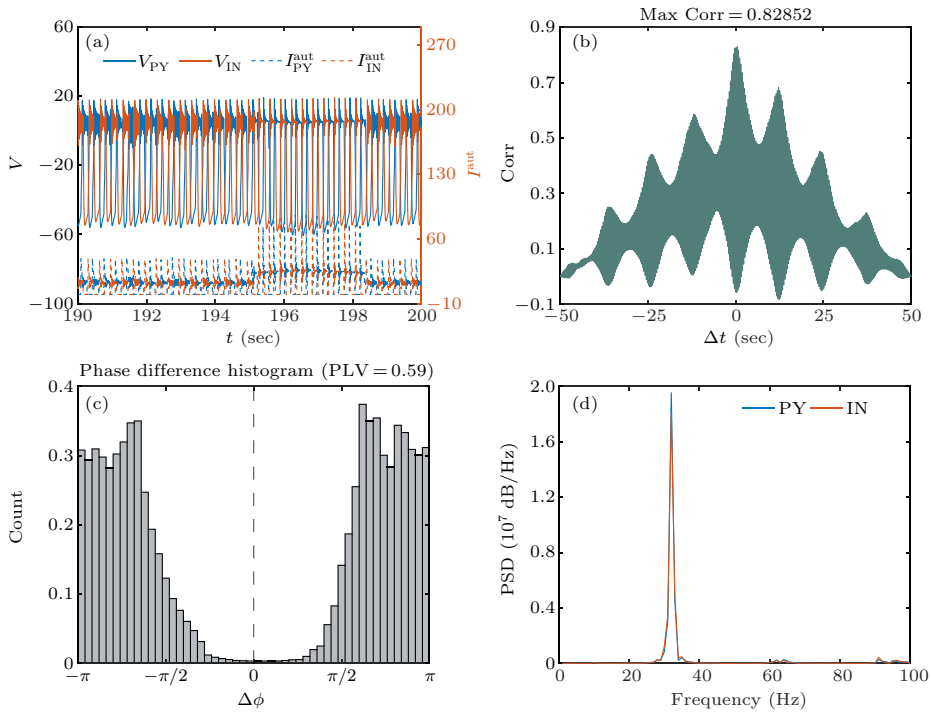


Fig. 6. No synchronization due to chaotic bursting at the time delay $\tau = 300$ ms for the excitatory autapse in the neuron–astrocyte network. (a) Time series of membrane potentials (V_{PY}, V_{IN}, solid lines) and corresponding autaptic currents (I^{aut}_{PY}, I^{aut}_{IN}, dashed lines) for the PY neuron (blue lines) and IN (orange lines). Both neurons exhibit complex chaotic bursting patterns. (b) The cross-correlation Corr(Δt) is calculated within a range of Δt from -50 s to 50 s to quantify the degree of lag synchronization. Although the maximum correlation reaches 0.82852, the overall fluctuation of the function between 0 and 0.8 indicates that lag synchronization is not verified. (c) Histogram showing the distribution of phase differences ($\Delta\varphi$) between PY and IN neurons. The bimodal distribution and a PLV of 0.59 confirm the absence of phase synchronization. (d) PSD curves for the PY and IN neurons. The coinciding PSD curves suggest that both neurons share identical statistical firing patterns despite the lack of temporal synchronization.

completely, as shown in Fig. 3(b), confirming the presence of lag synchronization. The statistical distribution of phase differences $\Delta\varphi$ in Fig. 3(c), along with a computed PLV = 0.78 from Eq. (30), indicates phase synchronization. Additionally, PSD plots of the two neurons in Fig. 3(d) display coinciding curves, further supporting this observation.

As τ increases to 10 ms, the two neurons achieve nearly complete synchronous bursting, as shown in Fig. 4(a). The lag $\Delta t = -0.0213$ s is very close to zero, so we shift the IN neuron as $V_{IN}(t) = V_{IN}(t - 0.0213)$ to make the time series fully overlap, as demonstrated in Fig. 4(b). These results confirm that lag synchronization evolves into nearly complete synchronization. Moreover, the concentrated phase differences and a computed PLV of 0.99 in Fig. 4(c) indicate robust phase synchronization. Finally, the identical PSD curves in Fig. 4(d) further validate matched firing patterns, providing strong evidence of nearly complete synchronization.

However, when the time delay τ reaches 186 ms, chaotic bursting patterns accompanied by irregular excitatory autaptic currents emerge in both the PY and IN neurons, resulting in the absence of synchronization, as shown in Fig. 5(a). As τ further increases to 300 ms, desynchronized chaotic bursting persists for both neurons, as illustrated in Fig. 6(a).

The lack of lag synchronization at $\tau = 186$ ms is evidenced by the cross-correlation function Corr(Δt) in Eq. (26), which fluctuates between 0 and 0.6 and returns to 0 over the range $\Delta t \in [-50, 50]$ s, with a maximum value of 0.56459, as shown in Fig. 5(b). Similarly, lag synchronization at $\tau = 300$ ms cannot be confirmed because Corr(Δt) varies between 0 and 0.8 and returns to 0 within the same Δt range, with a maximum of 0.82852 (Fig. 6(b)).

Phase synchronization is also absent at these delays, as indicated by the uniform distribution of phase differences $\Delta\varphi$ with PLV = 0.18 at $\tau = 186$ ms (Fig. 5(c)), and a bimodal distribution of $\Delta\varphi$ with PLV = 0.59 at $\tau = 300$ ms (Fig. 6(c)). Furthermore, the PSD curves diverge at $\tau = 186$ ms (Fig. 5(d)), highlighting distinct firing patterns, whereas at $\tau = 300$ ms the PSD curves coincide (Fig. 6(d)), indicating that the neurons share similar statistical firing patterns.

As the time delay τ increases to 500 ms, the neurons recover nearly complete synchronous bursting discharges, as shown in Fig. 7(a). The time series of the two neurons overlap upon applying a compensatory shift of $\Delta t = -0.0002$ s (Fig. 7(b)), confirming lag synchronization. The phase differences $\Delta\varphi$ form a single-peak distribution with PLV = 0.98 (Fig. 7(c)), indicating strong phase synchronization. The coinciding PSD curves (Fig. 7(d)) demonstrate identical firing patterns between the two neurons.

Overall, variation of the excitatory autaptic time delay τ in the neuron–astrocyte network drives the PY and IN neurons

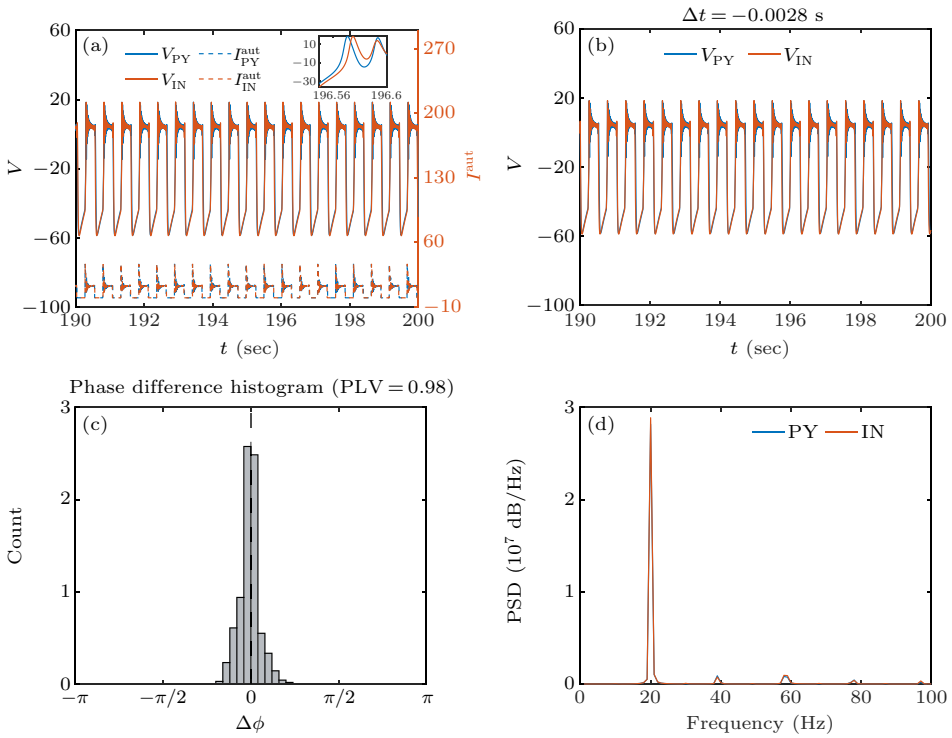


Fig. 7. Lag and phase synchronizations at the time delay $\tau = 500$ ms for the excitatory autapse in the neuron–astrocyte network. (a) Time series of membrane potentials (V_{PY}, V_{IN}, solid lines) and corresponding autaptic currents (I^{aut}_{PY}, I^{aut}_{IN}, dashed lines) for the PY neuron (blue lines) and IN (orange lines). The traces illustrate the restoration of near-complete synchronous bursting discharges. The inset provides a magnified view of the individual bursts to highlight the temporal alignment. (b) Temporal alignment of neuronal membrane potentials following a compensatory shift of $\Delta t = -0.0028$ s. The precise overlap of the traces demonstrates the existence of lag synchronization. (c) Histogram showing the distribution of phase differences ($\Delta\varphi$) between PY and IN neurons. The single-peak distribution centered at zero, with a PLV of 0.98, signifies robust phase synchronization. (d) PSD profiles for the PY and IN neurons. The coinciding curves and identical peak frequencies demonstrate that the neurons exhibit consistent firing patterns and spectral characteristics.

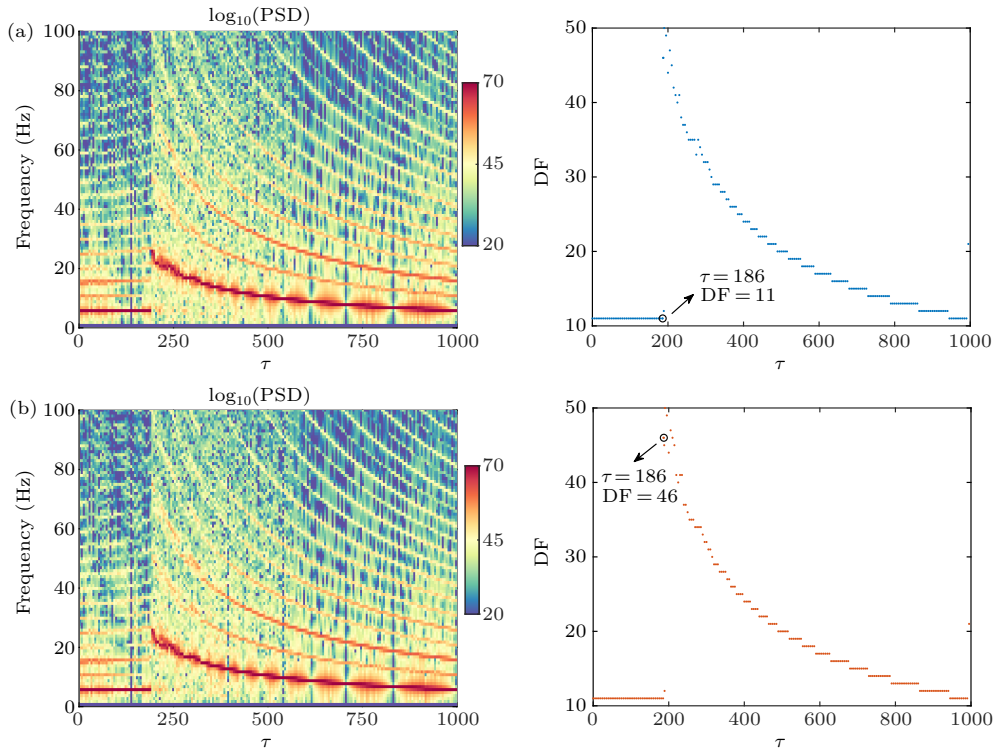


Fig. 8. PSD at different frequencies as well as the dominant frequency (DF) corresponding to the maximum PSD, with respect to the varying time delay τ of the excitatory autapse, for (a) the PY neuron and (b) the IN neuron in the neuron–astrocyte network. The heatmaps (left panels) display the $\log_{10}$(PSD) values across a frequency range of 0–1000 Hz as a function of the time delay τ. The corresponding scatter plots (right panels) track the DF at which the PSD is maximized. For $\tau < 186$ ms, both PY and IN neurons exhibit a stable DF. At the critical threshold of $\tau = 186$ ms, an abrupt shift in the spectral characteristics of the IN neuron occurs, with the DF increasing sharply. As τ increases beyond this threshold, the DF undergoes a stepwise decline.

from synchronized bursting to desynchronized chaotic bursting and back to synchronized bursting. To further illustrate the influence of τ, heatmaps of the PSD at different frequencies and the corresponding dominant frequency (DF) at the maximum PSD are plotted for the PY neuron (Fig. 8(a)) and the IN neuron (Fig. 8(b)). Additionally, PSD profiles at the fixed delays discussed in Figs. 3(d)–7(d) are included. When $\tau < 186$ ms, the DF (at the maximum of $10\log_{10}$PSD) remains nearly constant at 5 Hz for both neurons. Once τ exceeds 186 ms, the DF sharply increases to 20 Hz, followed by a stepwise decrease as τ further rises. The abrupt DF increase at $\tau \approx 186$ ms corresponds to the transition from synchronized to desynchronized bursting and aligns with the sudden decrease in inter-burst intervals (IBIs), as shown in Figs. 9(a) and 9(b).

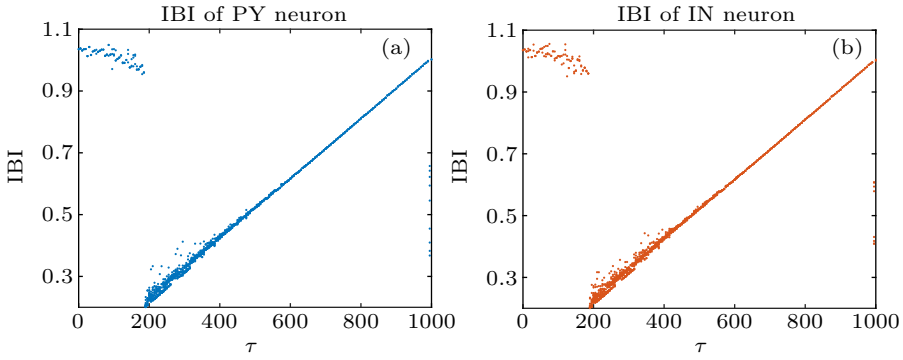


Fig. 9. Transition of inter-burst intervals (IBIs) in response to varying time delay τ of the excitatory autapse. The scatter plots illustrate the IBIs as a function of τ for (a) PY neurons and (b) IN. For $\tau < 186$ ms, both neurons exhibit relatively stable IBIs forming a plateau at higher values. At the critical threshold of approximately $\tau = 186$ ms, a prominent change occurs, where a sudden descent in the IBI is observed. Beyond this threshold, the IBI exhibits an approximately linear dependence on τ.

3.2. Synchronization of diverse bursting patterns followed by burst desynchronization induced by time delay of inhibitory autapse

We continue to investigate inhibitory autaptic modulation on the firing behaviors of PY and IN neurons by setting E_s in Eq. (24) to -60 mV, which is lower than the minimum voltage. Here, we select the values of the time delay τ of the inhibitory autapse as 0 ms, 20 ms, 100 ms, 500 ms, and 700 ms to explore lag and phase synchronizations of bursting for the PY and IN neurons in the neuron–astrocyte network.

At the time delay of $\tau = 0$ ms, the PY and IN neurons with the inhibitory autapse exhibit synchronization in "square-wave" bursting, as shown in Fig. 10(a). The inhibitory autaptic current sharply decreases, causing the membrane potential $V(t)$ to rise and the neuron to fire spikes. After multiple peaks, it starts to decline, leading the membrane potential $V(t)$ to decrease and the neuron to return to the rest state, thus completing a burst firing cycle. As the IN neuron fires ahead of the PY neuron in Fig. 10(a), we set $V_{\rm in}(t) = V_{\rm in}(t + 0.0729)$ for the IN neuron using the computed lag of $\Delta t = 0.0729$ s to make the time series of the two neurons overlap, as shown in Fig. 10(b), confirming lag synchronization between the PY and IN neurons. In addition, the statistical diagram of the phase difference $\Delta\varphi$ in Fig. 10(c) shows a single peak, with PLV $= 0.54$, indicating moderate phase synchronization. Figure 10(d) shows the PSD plots of the two neurons, where the PSD curves of the PY and IN neurons nearly overlap, further indicating consistent firing patterns between them.

As the time delay τ is increased to 20 ms, both PY and IN neurons fail to remain fully synchronized, although they exhibit nearly uniform bursting patterns characterized by high and low spike rates, as shown in Fig. 11(a). The computed lag $\Delta t = 0.2331$ s allows the time series of the two neurons to almost overlap, but the low spikes remain misaligned, as shown in Fig. 11(b), confirming incomplete lag synchronization between the PY and IN neurons. Besides, phase synchronization cannot be attained, since the statistical diagram of the phase difference $\Delta\varphi$ in Fig. 11(c) is approximately uniformly distributed with PLV $= 0.14$. Moreover, different peaks appear at the same frequency in the PSD plots for PY and IN neurons, as shown in Fig. 11(d), indicating that the two neurons exhibit similar firing patterns overall, but with differences in inter-burst intervals or peak amplitudes.

At the time delay $\tau = 100$ ms, both neurons exhibit "triangle" bursting with nearly complete synchronization as shown in Fig. 12(a). The time-series diagrams of the two neurons overlap with a lag of only $\Delta t = -0.0168$ s for the IN neuron in Fig. 12(b). Furthermore, the statistical diagram of phase differences shows a single-peak distribution with PLV $= 0.94$ in Fig. 12(c), indicating phase synchronization between the two neurons. Finally, the PSD curves of the PY and IN neurons coincide in Fig. 12(d), demonstrating that both neurons exhibit synchronized firing with identical firing patterns.

As the time delay τ increases to 200 ms, both neurons display slightly irregular bursting patterns in Fig. 13(a), resulting in larger inter-burst intervals at the early stage and smaller intervals at the later stage. With the computed lag $\Delta t = 0.9909$ s, several bursts of the two neurons do not overlap as shown in

Fig. 13(b), confirming incomplete lag synchronization. The phase difference $\Delta\varphi$ in Fig. 13(c) is approximately uniformly distributed between $-\pi$ and 0, with PLV = 0.66, indicating weak phase synchronization. In addition, differences in PSD peaks at different frequencies in Fig. 13(d) suggest distinct firing patterns between the two neurons.

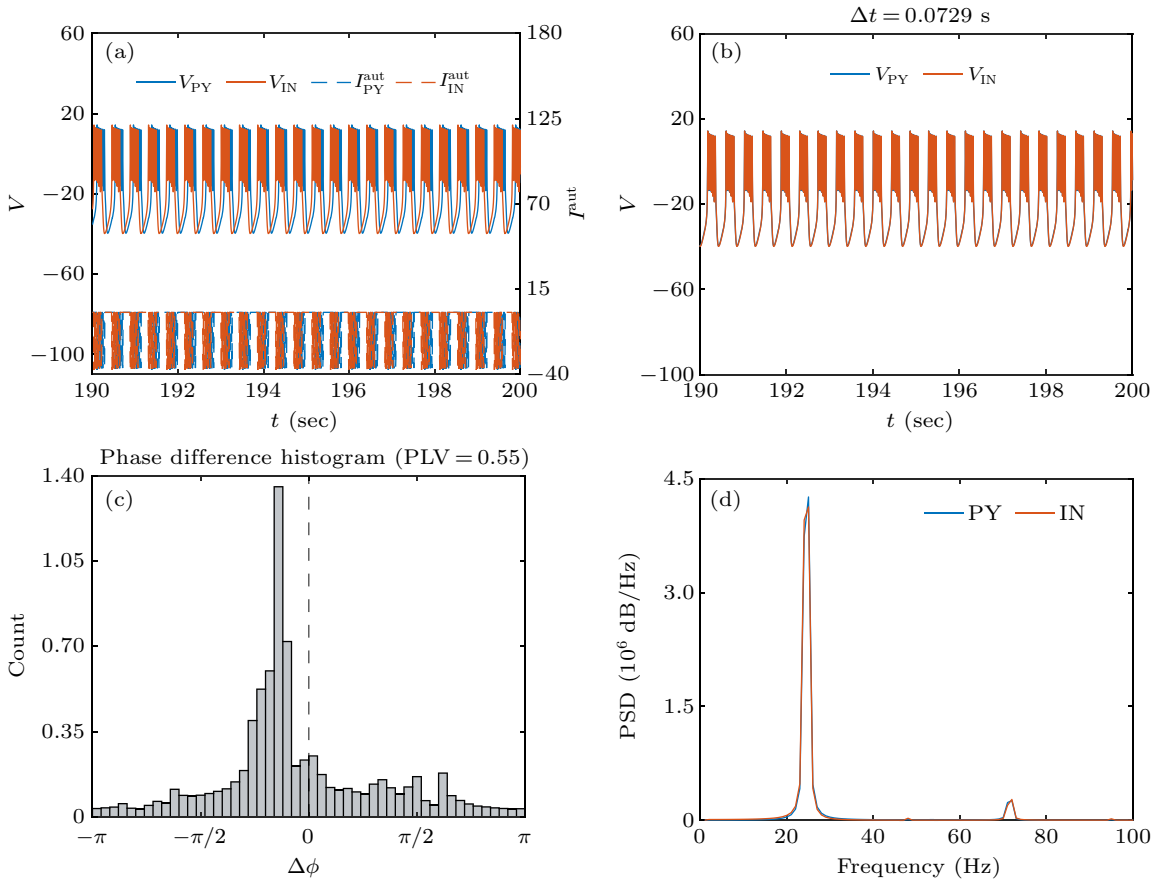


Fig. 10. Synchronization of inhibitory autaptic modulation-induced "square-wave" bursting in the neuron–astrocyte network for $\tau = 0$ ms. (a) Time series of membrane potentials (V_{PY}, V_{IN}, solid lines) and corresponding autaptic currents (I^{aut}_{PY}, I^{aut}_{IN}, dashed lines) for PY neuron (blue lines) and IN (orange lines). The sharp reduction in inhibitory autaptic current triggers the initiation of "square-wave" bursting, and the subsequent decline in current promotes the transition back to the quiescent state. (b) Temporal alignment of neuronal membrane potential following a compensatory shift of $\Delta t = 0.0729$ s, which corresponds to the time lag at which the cross-correlation function is maximized. The overlap of the two trajectories confirms the emergence of lag synchronization between the PY and IN neurons. (c) Histogram showing the distribution of phase differences ($\Delta\phi$) between PY and IN neurons. The presence of a prominent single peak and a PLV of 0.54 indicates a state of moderate phase synchronization. (d) PSD curves for the PY and IN neurons. The nearly overlapping PSD curves further demonstrate the consistent firing patterns between the PY and IN neurons.

At $\tau = 500$ ms, both neurons exhibit synchronous "Valley-shaped" bursting with sharply reduced inter-burst intervals as shown in Fig. 14(a). Following a very small lag of $\Delta t = -0.0175$ s for the IN neuron, the time-series diagrams overlap, confirming lag synchronization in Fig. 14(b). The statistical diagram of phase differences in Fig. 14(c) presents a single-peak distribution with PLV = 0.99, indicating strong phase synchronization. Figure 14(d) shows coinciding PSD curves for the PY and IN neurons, demonstrating identical firing patterns.

As the time delay τ reaches 700 ms, both neurons exhibit slightly irregular bursting patterns, resulting in larger inter-burst intervals at the early stage and smaller intervals at the later stage in Fig. 15(a). Following a lag of $\Delta t = 0.571$ s for the IN neuron, the time-series diagrams mostly overlap, confirming nearly lag synchronization in Fig. 15(b). However, the phase difference $\Delta\varphi$ with PLV = 0.81 in Fig. 15(c) is approximately uniformly distributed between $-\pi$ and 0, indicating weak phase synchronization. Moreover, differences in PSD peaks at different frequencies in Fig. 15(d) suggest distinct firing patterns between the two neurons.

The increase in the time delay τ for the inhibitory autapse in the neuron–astrocyte network leads to synchronization behaviors of diverse bursting patterns followed by burst desynchronization for the PY and IN neurons. We further illustrate the transition of bursting patterns over a range of time delays τ by computing the PSD over a frequency range from 0 to 100 Hz as well as the dominant frequency (DF) at the maximum of the PSD, for the PY and IN neurons depicted in Fig. 16(a) and 16(b), respectively. As the time delay τ increases, multiple PSD peaks at different frequencies indicate the presence of firing patterns with more than one peak.

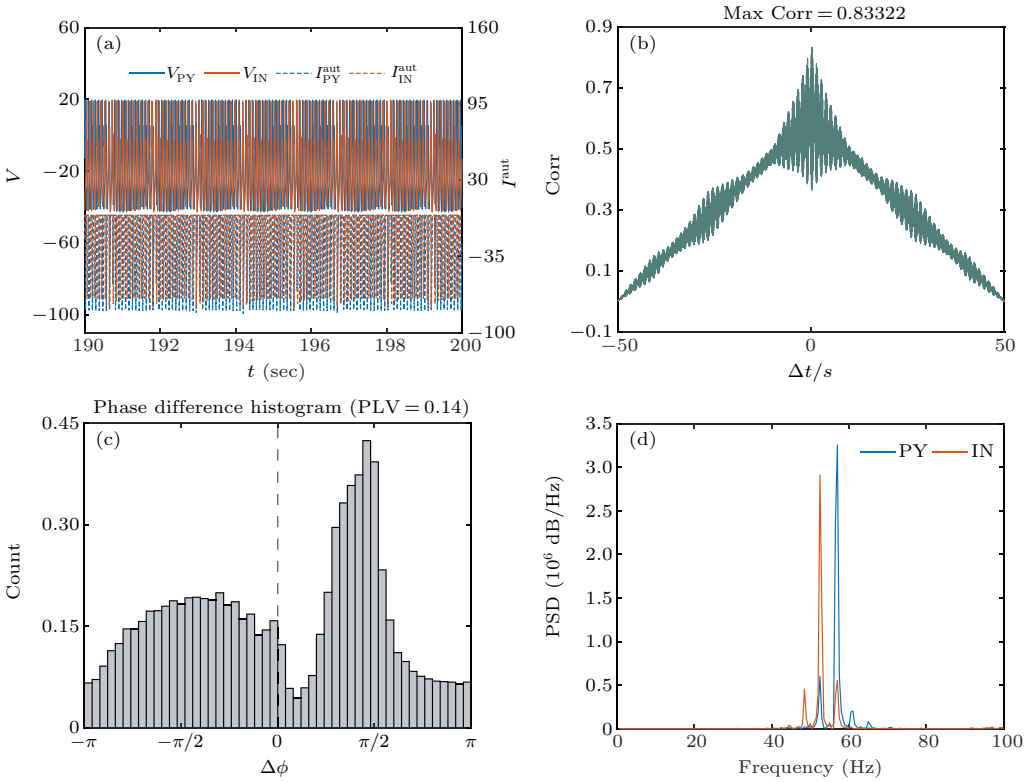


Fig. 11. Burst desynchronization due to the inhibitory autapse for $\tau = 20$ ms in the neuron–astrocyte network. (a) Time series of membrane potentials (V_{PY}, V_{IN}, solid lines) and corresponding autaptic currents (I^{aut}_{PY}, I^{aut}_{IN}, dashed lines) for PY neuron (blue lines) and IN (orange lines). Both neurons exhibit nearly uniform bursting patterns. (b) The cross-correlation Corr(Δt) is calculated within a range of Δt from -50 s to 50 s to quantify the degree of lag synchronization. The computed lag $\Delta t = 0.8332$ s indicates incomplete lag synchronization. (c) Histogram showing the distribution of phase differences ($\Delta\phi$) between PY and IN neurons. The approximately uniform distribution with PLV = 0.14 indicates lack of phase synchronization. (d) PSD curves for the PY and IN neurons. Although the primary peaks appear at identical frequencies, the differences in peak magnitudes and inter-burst intervals reflect the desynchronized state of the coupled system.

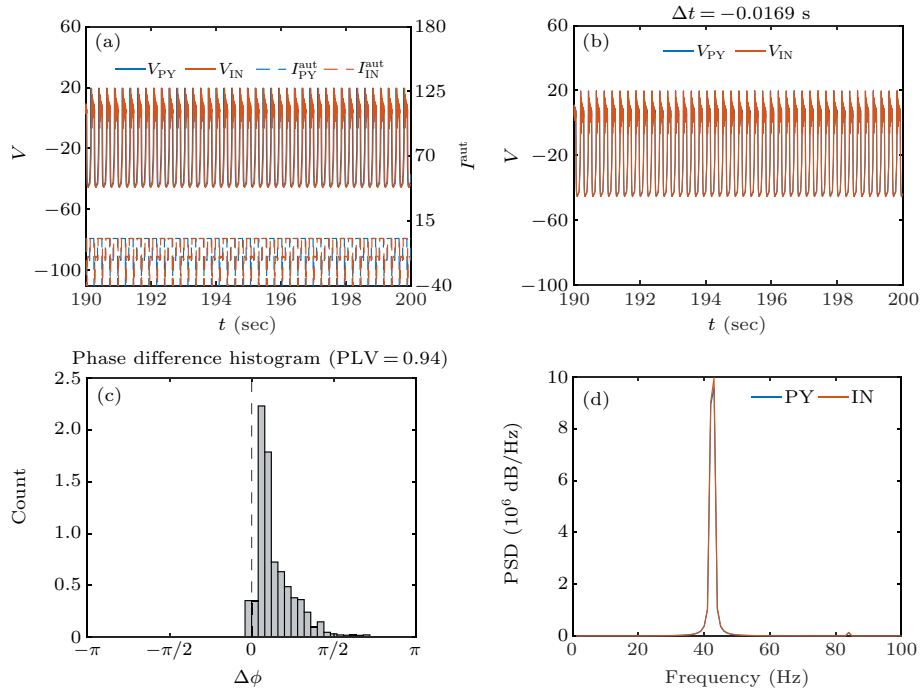


Fig. 12. Synchronization of "tapered" bursting in the neuron–astrocyte network with the inhibitory autapse for $\tau = 100$ ms. (a) Time series of membrane potentials (V_{PY}, V_{IN}, solid lines) and corresponding autaptic currents (I^{aut}_{PY}, I^{aut}_{IN}, dashed lines) for PY neuron (blue lines) and IN (orange lines). Both neurons exhibit characteristic "tapered" bursting patterns. (b) Temporal alignment of neuronal membrane potential following a compensatory shift of $\Delta t = -0.0169$ s. The nearly perfect overlap of the time series demonstrates a high degree of lag synchronization. (c) Histogram showing the distribution of phase differences ($\Delta\phi$) between PY and IN neurons. The distribution exhibits a prominent single peak centered near zero, and the PLV is 0.94, indicating robust phase synchronization. (d) PSD curves for the PY and IN neurons. The overlapping PSD peaks indicate that both neurons maintain identical firing frequencies and synchronized oscillatory regimes.

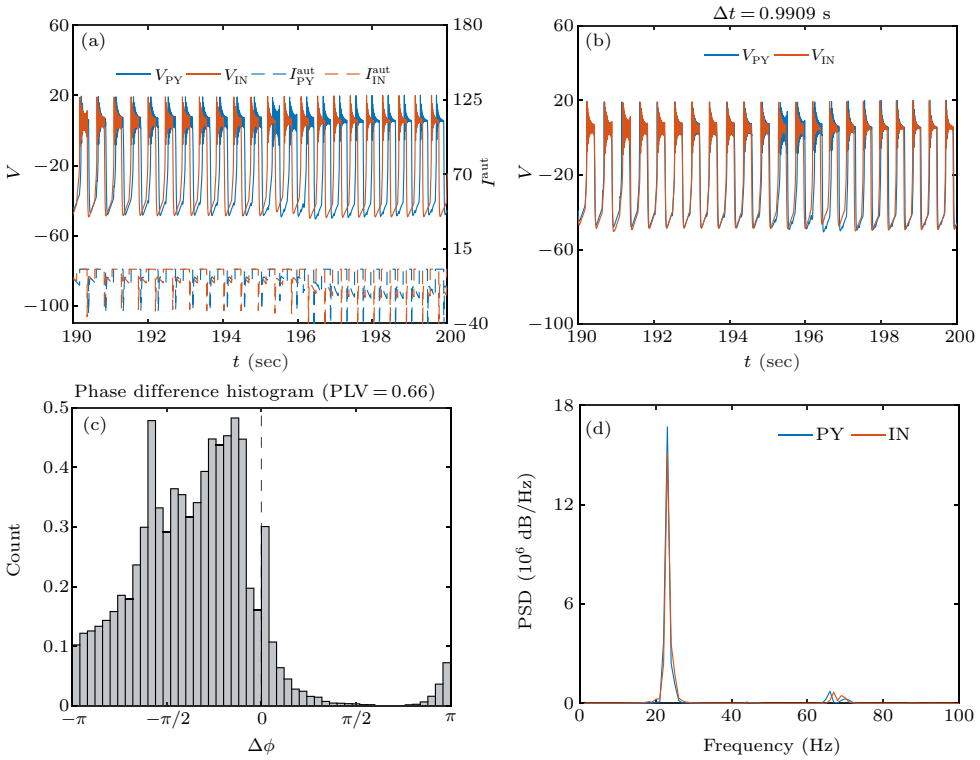


Fig. 13. Burst desynchronization due to the inhibitory autapse for $\tau = 200$ ms in the neuron–astrocyte network. (a) Time series of membrane potentials (V_{PY}, V_{IN}, solid lines) and corresponding autaptic currents (I^{aut}_{PY}, I^{aut}_{IN}, dashed lines) for PY neuron (blue lines) and IN (orange lines). Both neurons exhibit irregular bursting patterns. (b) Temporal alignment of neuronal membrane potential following a compensatory shift of $\Delta t = 0.9909$ s. The misalignment of several bursts confirms incomplete lag synchronization between the PY and IN neurons under these delayed inhibitory conditions. (c) Histogram showing the distribution of phase differences ($\Delta\phi$) between PY and IN neurons. The distribution is approximately uniform, with a PLV of 0.66, indicating weak phase synchronization. (d) PSD curves for the PY and IN neurons. Discrepancies in the PSD peaks further indicate divergence in the firing patterns and the resulting desynchronization.

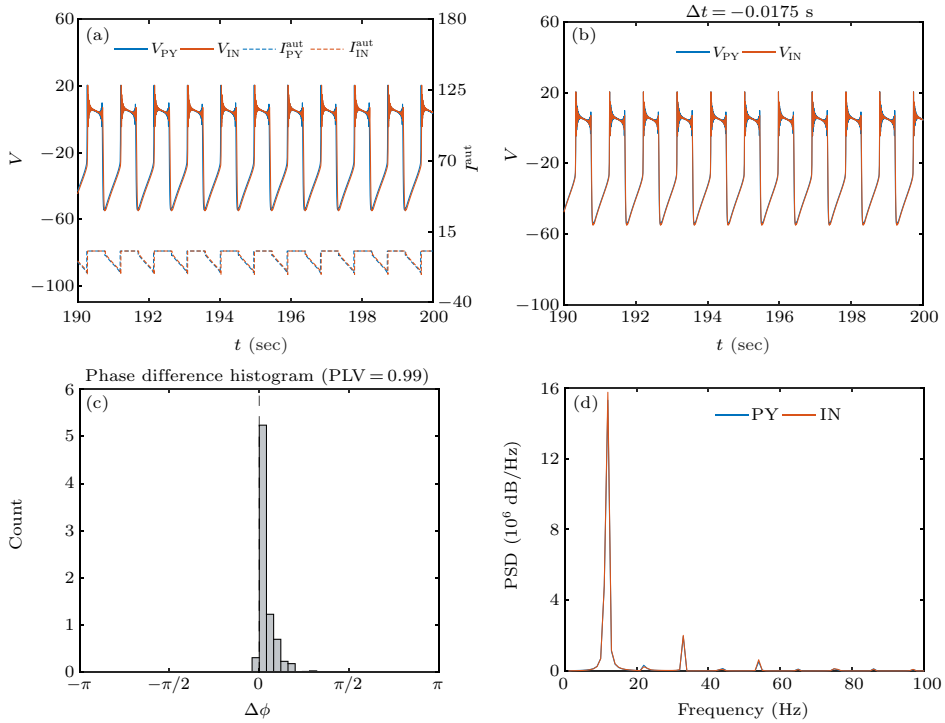


Fig. 14. Synchronization of "Valley-shaped" bursting in the neuron–astrocyte network with the inhibitory autapse for $\tau = 500$ ms. (a) Time series of membrane potentials (V_{PY}, V_{IN}, solid lines) and corresponding autaptic currents (I^{aut}_{PY}, I^{aut}_{IN}, dashed lines) for PY neuron (blue lines) and IN (orange lines). Both neurons exhibit synchronized "Valley-shaped" bursting patterns with sharply reduced inter-burst intervals (IBIs). (b) Temporal alignment of neuronal membrane potential following a compensatory shift of $\Delta t = -0.0175$ s, confirming the emergence of lag synchronization. (c) Histogram showing the distribution of phase differences ($\Delta\phi$) between PY and IN neurons. The distribution exhibits a prominent single-peak profile with a PLV of 0.99, demonstrating robust phase synchronization. (d) PSD curves for the PY and IN neurons. Coinciding PSD curves indicate identical firing patterns and spectral characteristics between the two neurons under the specified time delay.

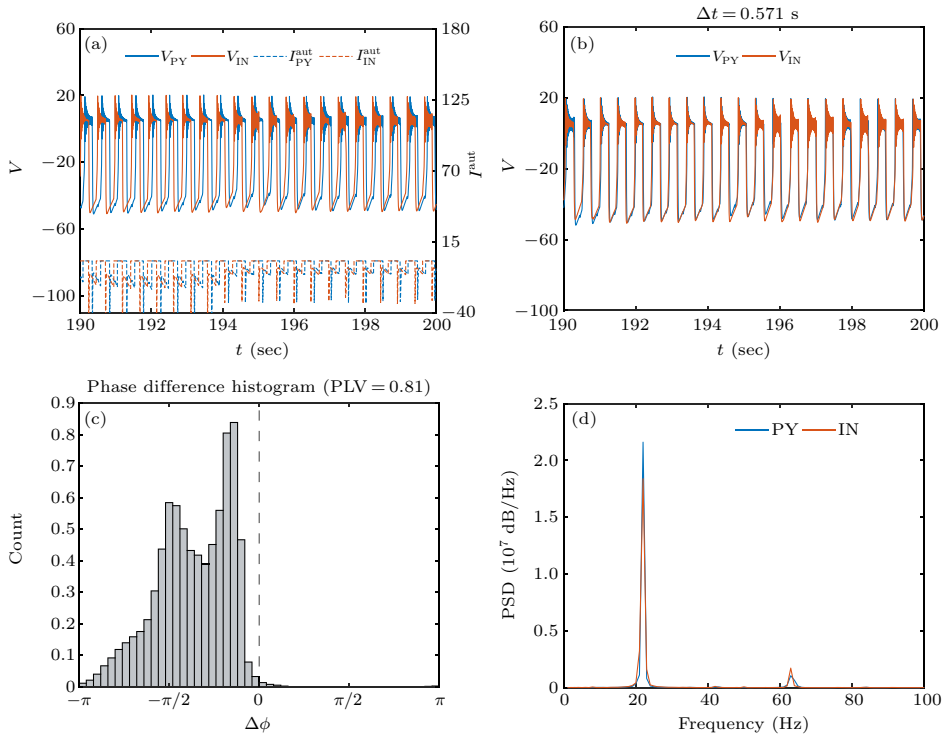


Fig. 15. Burst desynchronization due to the inhibitory autapse for $\tau = 700$ ms in the neuron–astrocyte network. (a) Time series of membrane potentials (V_{PY}, V_{IN}, solid lines) and corresponding autaptic currents (I^{aut}_{PY}, I^{aut}_{IN}, dashed lines) for PY neuron (blue lines) and IN (orange lines). Both neurons exhibit irregular, non-uniform bursting patterns. (b) Temporal alignment of neuronal membrane potential following a compensatory shift of $\Delta t = 0.571$ s. The substantial overlap between the two traces indicates nearly complete lag synchronization despite the inherent irregularity of the bursts. (c) Histogram showing the distribution of phase differences ($\Delta\phi$) between PY and IN neurons. The PLV of 0.81 and the approximately uniform distribution of $\Delta\varphi$ within the interval $[-\pi, 0]$ suggest a state of weak phase synchronization. (d) PSD curves for the PY and IN neurons. Mismatched PSD peak frequencies indicate that the two neurons maintain distinct firing patterns and periodicities under these conditions.

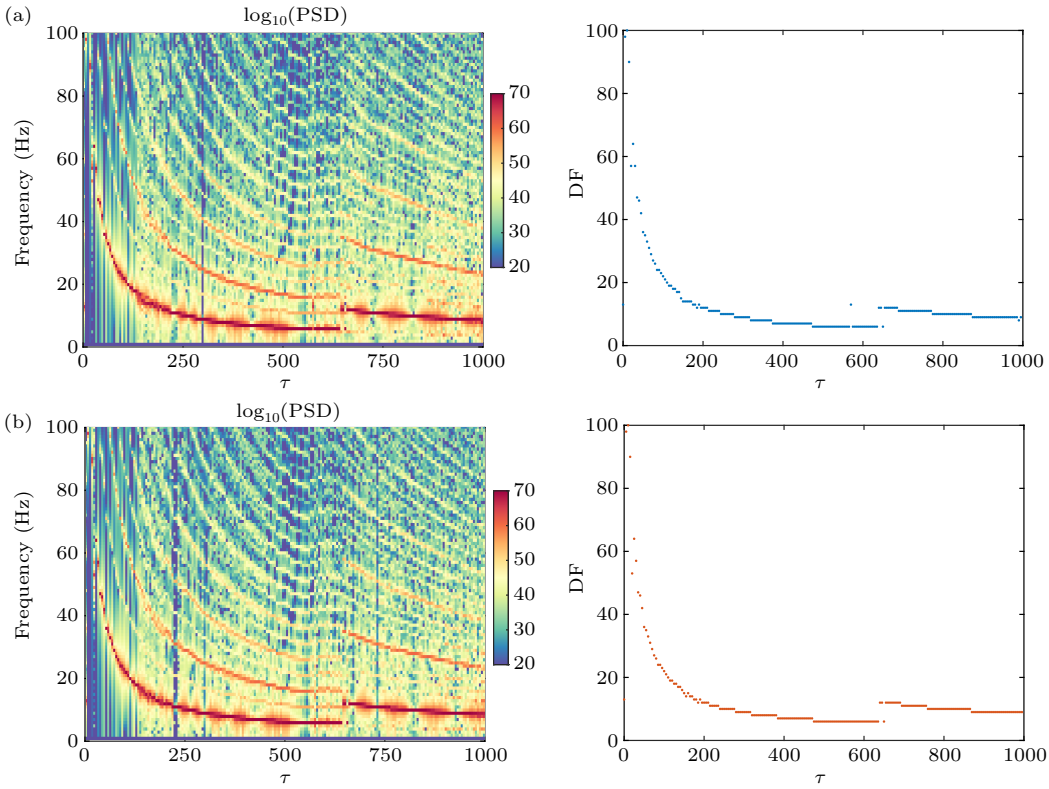


Fig. 16. PSD at different frequencies as well as dominant frequency (DF) at the maximum of the PSD, with respect to the varying time delay τ of the inhibitory autapse, for (a) the PY neuron and (b) the IN neuron in the neuron–astrocyte network. (a) The heatmaps (left panels) display the $\log_{10}$(PSD) values across a frequency range of 0–1000 Hz as a function of the inhibitory autaptic time delay τ. (b) The corresponding scatter plots track the dominant frequency (DF) at which the PSD is maximized. These results demonstrate that increasing the inhibitory autaptic time delay τ induces complex transitions in the bursting patterns of both neurons.

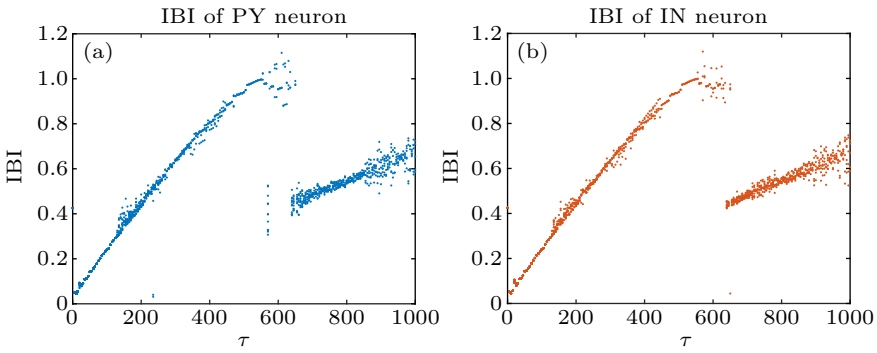


Fig. 17. Transition of inter-burst intervals (IBIs) in response to varying inhibitory autaptic time delay. The scatter plots illustrate the IBIs as a function of the time delay τ of the inhibitory autapse for (a) PY neurons and (b) IN. For $\tau < 600$ ms, the IBIs exhibit a nearly linear monotonic increase. At the critical transition point at $\tau \approx 650$ ms, a distinct discontinuity is observed, at which the IBI values undergo a sharp decrease.

Notably, within the time delay range of 500–650 ms, a horizontal band of non-zero PSD values is observed, implying consistent firing behaviors in the coupled system. The breakpoint in the PSD curve as well as the abrupt increase of the DF occurs at $\tau = 650$ ms. Then, as τ exceeds 650 ms, the fluctuation range of the PSD and dominant frequency slightly decreases, consistent with the firing characteristics observed at specific time delays described earlier. To better understand the impact of the time delay τ on bursting behavior under inhibitory autaptic conditions, the inter-burst intervals (IBIs) for varying τ are plotted in Fig. 17. As diverse neuronal bursting patterns emerge, the IBIs of both neurons exhibit a steep decrease followed by slight increases after about $\tau = 650$ ms, which aligns with the characteristics discussed above.

4. Discussion

Autapses and astrocytes, as essential components of the central nervous system, play a pivotal role in regulating neuronal firing dynamics and merit in-depth investigation. In this study, we constructed a minimal neuronal network comprising PY and IN neurons modulated by astrocytes and incorporated time-delayed excitatory or inhibitory autapses to elucidate how autaptic time delay modulates the synchronization of neuronal firing behaviors. Our results demonstrate that both excitatory and inhibitory autapses can alter neuronal firing activities within the neuron–astrocyte network and tune synchronization phenomena. Specifically, varying the time delay of excitatory autapses induces a transition of firing patterns in PY and IN neurons from synchronized bursting, through desynchronized chaotic bursting, back to synchronized bursting. In contrast, increasing the time delay of inhibitory autapses triggers a sequence of synchronization transitions among diverse bursting patterns, followed by burst desynchronization in PY and IN neurons. These findings provide valuable insights into the synergistic effects of autapses and glial cells in neural networks. However, this study is constrained by its focus on a minimal network of two neurons coupled to a single astrocyte, which lays the foundation for future investigations into autaptic functions in more complex neuron–astrocyte network architectures.

Acknowledgment

Project supported by the National Natural Science Foundation of China (Grant No. 12372060).

References

[1] Guan L, Gu H and Zhang X 2024 *Front. Comput. Neurosci.* **18** 1303925
[2] Palabas T and Yilmaz E 2025 *Nonlinear Dyn.* **113** 8991
[3] Kang J, Jiang L, Goldman S A and Nedergaard M 1998 *Nat. Neurosci.* **1** 683
[4] Zhao J, Fan D, Wang Q and Wang Q 2021 *Nonlinear Dyn.* **103** 913
[5] Ji Q, Qie X and Ye M 2023 *Nonlinear Dyn.* **111** 7713
[6] Jha M K, Jo M, Kim J H and Suk K 2019 *Neuroscientist* **25** 227
[7] Erkan E 2023 *Chaos Solitons Fractals* **177** 114223
[8] Erkan Y, Sarac Z and Yilmaz E 2019 *Nonlinear Dyn.* **95** 3411
[9] Pankratova E V, Kalyakulina A I, Stasenko S V, Gordleeva S Y, Lazarevich I A and Kazantsev V B 2019 *Nonlinear Dyn.* **97** 647
[10] Stogsdill J A, Ramirez J, Liu D, Kim Y H, Baldwin K T, Enustun E, Ejikeme T, Ji R R and Eroglu C 2017 *Nature* **551** 192
[11] Ioannou M, Jackson J, Sheu S, Chang C, Weigel A, Liu H, Pasolli H, Xu C, Pang S and Matthies D 2019 *Cell* **177** 1522
[12] Haydon P G 2006 *Physiol. Rev.* **86** 1009
[13] Volterra A, De Pitta M and Brunel N 2016 *Neuroscience* **323** 43
[14] Van der Loos H and Glaser E M 1972 *Brain Res.* **48** 355
[15] Yang Y, Li Y, Gu H and Qi C 2023 *Nonlinear Dyn.* **111** 7751
[16] Zhao Z, Li L and Gu H 2020 *Commun. Nonlinear Sci. Numer. Simul.* **85** 105250
[17] Song X, Wang H and Chen Y 2019 *Nonlinear Dyn.* **96** 2341
[18] Baysal V, Erkan E and Yilmaz E 2021 *Philos. Trans. R. Soc. A* **379** 20200237
[19] Guo S, Tang J, Ma J and Wang C 2017 *Complexity* **2017** 1
[20] Aghababaei S, Balaraman S, Rajagopal K, Parastesh F, Panahi S and Jafari S 2021 *Chaos Solitons Fractals* **153** 111498
[21] Zhang N, Li D and Xing Y 2021 *Eur. Phys. J. B* **94** 1
[22] Parthasarathy S, Parastesh F, Natiq H, Rajagopal K and Jafari S 2023 *Complexity* **2023** 1
[23] Makovkin S Y, Shkerin I V, Gordleeva S Y and Ivanchenko M V 2020 *Chaos Solitons Fractals* **138** 109951
[24] Motter A E 2012 *Nat. Phys.* **6** 164
[25] Bao B, Yang Q, Zhu L, Bao H, Xu Q, Yu Y and Chen M 2019 *Int. J. Bifurcat. Chaos* **29** 1950134
[26] Amiri M, Hosseinmardi N, Bahrami F and Janahmadi M 2013 *J. Comput. Neurosci.* **34** 489
[27] Tang J, Luo J M and Ma J 2013 *PLoS One* **8** e80324
[28] Li Y X and Rinzel J 1994 *J. Theor. Biol.* **166** 461
[29] Tsumoto K, Kitajima H, Yoshinaga T, Aihara K and Kawakami H 2006 *Neurocomputing* **69** 293
[30] Rybalova E, Strelkova G, Schöll E and Anishchenko V 2020 *Chaos* **30** 061104

[31] Della Rossa F, Pecora L, Blaha K, Shirin A, Klickstein I and Sorrentino F 2020 *Nat. Commun.* **11** 3179
[32] Andrzejak R G, Ruzzene G, Malvestio I, Schindler K, Schöll E and Zakharova A 2018 *Chaos* **28** 091101
[33] Ibrahim M M, Kamran M A, Mannan M M N, Jung I H and Kim S 2021 *Sci. Rep.* **11** 3884
[34] Vivekanandhan G, Mehrabbeik M, Natiq H, Hatef B, Merrikhi Y and Jafari S 2023 *Pramana* **97** 171
[35] Sakkalis V 2011 *Comput. Biol. Med.* **41** 1110
[36] Yilmaz E, Ozer M, Baysal V and Perc M 2016 *Sci. Rep.* **6** 30914
[37] Baysal V and Calim A 2023 *Chaos Solitons Fractals* **175** 114059
[38] Baysal V, Erkan E and Yilmaz E 2021 *Philos. Trans. R. Soc. A* **379** 20200237
[39] Jiang H J, Aćimović J, Manninen T, Ahokainen I, Stapmanns J, Lehtimäki M, Savin T, Poranen M, Kiviniemi V, Hyttinen J, Zhigalov A, Palva S and Palva J M 2025 *PLoS Comput. Biol.* **21** e1013503
[40] Gordleeva S Y, Pankratova E V, Kalyakulina A I, Lazarevich I A and Kazantsev V B 2021 *Front. Cell. Neurosci.* **15** 631485
[41] Apata C O, Usman S, Ojo J O, Ogundare S O, Olanrewaju S T, Ajibola S O, Abioye T O and Abdullahi I A 2024 *Chin. Phys. B* **33** 058704